Research papers

Investigating the performance of data mining, lumped, and distributed models in runoff projected under climate change

Seyedeh Hadis Moghadam [a], Parisa-Sadat Ashofteh [a,*], Hugo A. Loáiciga [b]

[a] *Department of Civil Engineering, University of Qom, Qom, Iran*
[b] *Department of Geography, University of California, Santa Barbara, CA, USA*

ARTICLE INFO

ABSTRACT

This work evaluates the effects of climate change on the surface water resources (river flow) of the Sanjabi basin, Iran, by comparing data-mining, lumped, and distributed models, namely artificial neural networks (ANN), the identification of unit hydrographs and component flows from rainfall, evaporation, and streamflow (IHACRES) model, and the soil and water assessment tool (SWAT). Climate projections in terms of monthly temperature and rainfall made by 17 atmosphere–ocean general circulation models (AOGCMs) by the 5th Assessment Report (AR5) of the Intergovernmental Panel on Climate Change (IPCC) under emission scenarios of Representative Concentration Pathways (RCPs) (RCP2.6, RCP4.5, and RCP8.5) during the baseline period 1971–2000 and future periods 2040–2069 and 2070–2099 are applied in the Sanjabi basin. The predictive skill of the AOGCMs is evaluated with performance criteria. The evaluation results indicate the CNRM-CM5 model features the best performance in terms of rainfall, average temperature, and minimum temperature projections, and the GFDL-CM3 provides the most accurate maximum temperature projections. Four downscaling methods (change factor (Delta), ClimGEN, LARS-WG, and Genetic Programming (GP)) are compared based on the R^2, *RMSE*, *MAE,* and *NSE*. The predictive skill of the LARS-WG method was the highest. ANN, IHACRES, and SWAT are implemented to project future runoff following calibration and testing. The IHACRES model exhibits the best performance. The IHACRES model is applied to project future runoff under climate-change scenarios. The results indicate a reduction in runoff under all emission scenarios in the two future periods, with the RCP8.5 scenario featuring the largest reductions in runoff in 2040–2069 and 2070–2099 and being equal to 42.0 and 44.3%, respectively.

1. Introduction

Increasing burning of fossil fuels for energy generation, on the one hand, and deforestation and environmental degradation, on the other hand, have led to an increase in greenhouse gases and rising surface air temperature. The alteration of the earth-atmosphere radiation balance has modified climatic patterns, which is suspected of altering the intensity, duration, and frequency of precipitation, and poses challenges to the utilization of water resources and agriculture in many parts of the world (Vanuytrecht et al., 2012). The IPCC (2001) reported that the average global air surface temperature has risen since 1861 through present time by 0.6 ± 0.2 °C. Temperate increases are predicted to continue unless greenhouse gases concentrations are reduced (IPCC, 2021). Various studies have simulated the effects of climate change on the hydrologic cycle and compared the performance of models applied for this purpose. A brief review of studies reporting hydrologic simulations under climate-change conditions is presented next.

Afinowicz et al. (2005) implemented the SWAT to evaluate the influence of woody plants on the water budgets in the semi-arid, karstic, basin of the Guadalupe River in Texas, United States. Li et al. (2007) applied the SWAT in a basin of West Africa and showed that changing areas covered with forest, grassland, and savanna to agricultural lands or urban areas changed the natural hydrological conditions in the basin. Abbaspour et al. (2007) implemented the SWAT to simulate processes affecting water quantity, sediment transport, and nutrient loads in the Thur River basin (Switzerland). Mishra et al. (2007) used the SWAT to assess surface runoff and sediment transport from the 17 km^2 Banha watershed located in northeast India on a daily and monthly scale. Rostamian et al. (2008) applied the SWAT to assess runoff and sediment transport in the Beheshtabad (3860 km^2) watershed in the northern Karun basin in central Iran. Ustoorikar and Deo (2008) applied genetic programming (GP) in-filling of missing information about wave height
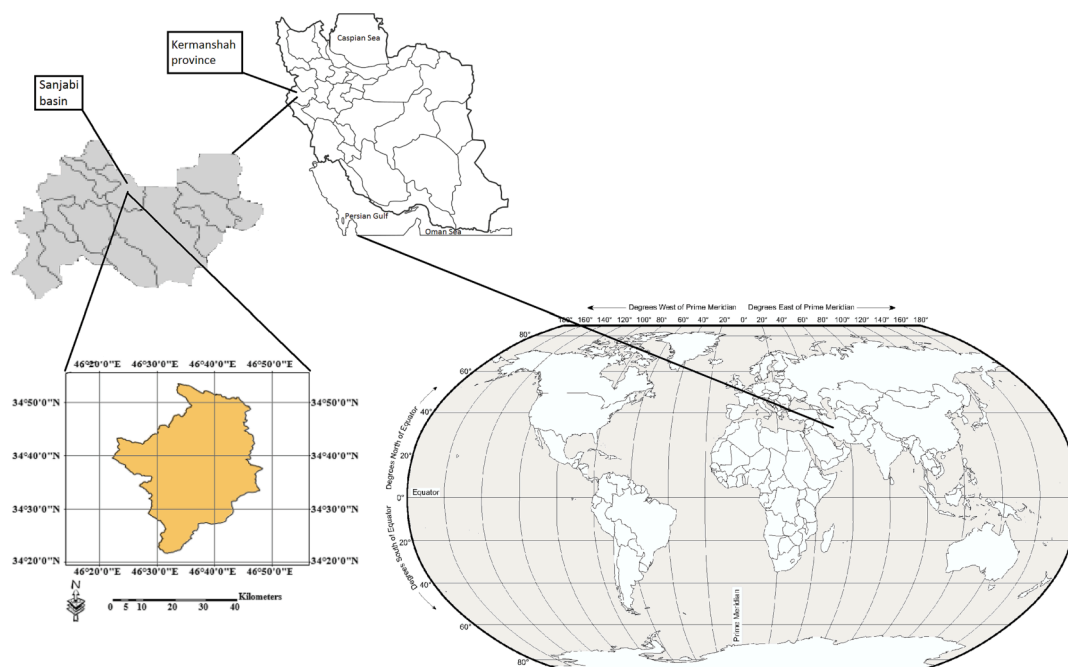
Fig. 1. Location of the Sanjabi (Bottom left) in Iran and Kermanshah province (top left).

in the Gulf of Mexico. Aytek and Kisi (2008) implemented GP for the explicit formulation of the daily suspended sediment–discharge relationship in the Tongue River in the state of Montana, United States. Vale and Holman (2009) provided an improved strategy for the future hydrologic management of the Bosherston Lakes in west Wales, England, and demonstrated the applicability of the SWAT in simulating karstic systems. Guven (2009) implemented linear genetic programming (LGP) and two versions of Neural Networks (NNs) in predicting time-series of daily flow rates at a station on the Schuylkill River at Berne, Pennsylvania, USA. Jeong et al. (2010) presented the development and testing of a sub-hourly rainfall-runoff model in SWAT. Sommerlot et al. (2013) compared three watershed-scale models, namely the SWAT, the High Impact Targeting (HIT) model, and the Revised Universal Soil Loss Equation (RUSLE2) model with the P-factor and R-factor performance criteria. Their results demonstrated the SWAT was the most accurate among the compared models, while HIT was the least accurate. Nikolaidis et al. (2013) modified the SWAT to simulate the hydrologic and chemical response of karstic systems. They evaluated the impacts of land use management and climate change in a Mediterranean watershed in Crete, Greece. Lin et al. (2015) conducted an investigation of runoff responses using the SWAT on Jinjiang, a coastal basin of southeastern China. Zuo et al. (2016) assessed the impacts of land use and climate changes on water and sediment yields in the Huangfuchuan River basin (HFCRB) by means of the SWAT. Ashofteh et al. (2016) developed comparative strategies for managing water demand under climate change conditions in the Aidoghmoush Basin in East Azerbaijan, Iran.

They implemented the IHACRES model for simulating runoff. Sarzaeim et al. (2017) proposed data-mining algorithms for runoff projection under climate change conditions. Moghadam et al. (2019) assessed the impact of climate change uncertainties on the Khorramabad River basin's runoff in Lorestan Province, Iran, applying the IHACRES model for simulating streamflow.

Forecasting and modeling temperature, precipitation, and runoff to determine the impact of climate change on water resources is necessary for planning the future management of water resources. The type of models used affects the accuracy of the modeling results. Previous comparison works have not evaluated the predictive skill of several hydrological models applied under climatic conditions, nor the uncertainties stemming from temperature and rainfall downscaling. It is, however, necessary to consider these uncertainties to choose the best model for a specific area application. Therefore, this paper introduces four methods, namely the Change Factor, LARS-WG, ClimGen, and GP for downscaling the temperature and rainfall obtained from the fifth report of IPCC have been compared. Also, this study presents a novel comparison of ANN, IHACRES, and SWAT, which are data-mining, lumped, and distributed models, respectively, with the purpose of assessing their accuracy in projecting runoff under climate-change conditions.

2. Methodology

The following sections describe (i) the study area, (ii) several greenhouse gases scenarios entertained in this work (this stage involves assessing the performance of 17 AOGCMs and choosing the best one), (iii) the selection of the method for downscaling rainfall and temperature data from alternative AOGCM models (this step applies the change factor, ClimGEN, LARS-WG, and GP methods, and the best model is chosen based on performance criteria), and (iv) the application and comparison of the ANN, IHACRES, and SWAT models for runoff projection in the periods 2040–2069 and 2070–2099."

2.1. The study area

The Sanjabi basin, with an areal extent of 1230 km^2, lies within Kermanshah province, Iran, as depicted in Fig. 1. Kermanshah province

Table 1
Specifications of meteorological and hydrometric stations located in the study area.

Type of station	Geographic characteristics			Station name	Number
	Elevation (m)	Latitude	Longitude		
Hydrometric	1339	34–33	46–47	Doab Merek	1
Rain gauge	1520	34–20	46–25	Gahvareh	2
Rain gauge	1490	34–39	46–36	Nahrabi	3
Synoptic	1363	34–43	46–40	Ravansar	4
Rain gauge	1318	34–35	47–15	Kermanshah	5
Rain gauge	1375	34–76	46–50	Javanrood	6

is surrounded by Kurdistan province to the north, Lorestan and Ilam provinces to the south, Hamedan province to the east, and Iraq to the west. The Sanjabi region is one of the sub-basins of the Karkheh River basin. The main river in the Sanjabi basin is the Merck River. The highest and lowest elevations in the Sanjabi basin equal 2800 and1307 m, respectively.

This study used monthly runoff data gathered at the Doab-Merek and Qarasu hydrometric stations, and rainfall, surface air temperature, and other daily meteorological data collected at selected meteorological and synoptic stations within the study area. Table 1 outlines the specifications of the stations. The precipitation, maximum temperature, and minimum temperature were used in the period 1971–2000. For the SWAT, wind speed, relative humidity, and daily insolation hours are required. The SWAT simulated these variables at stations where data were not available for stations during the baseline period (1971–2000).

2.2. Creating future climate scenarios

Atmospheric-Ocean general circulation model (AOGCMs) simulate the earth's climate system (Lane et al., 1999; Mitchell, 2003; Wilby and Harris, 2006). The 17 models applied in the IPCC-AR5 climate change simulation were considered in this work, namely, BCC-CSM1.1, BCC-CSM1.1(m), BNU-ESM, CanESM2, CCSM4, CESM1(CAM5), CNRM-CM5, GFDL-CM3, GFDL-ESM2G, GISS-E2-H, GISS-E2-R, MIROC5, MIROC-ESM, MIROC-ESM-CHEM, MPI-ESM-LR, MPI-ESM-MR, and NorESM1-M.

2.3. Non-climatic scenarios (emission scenarios)

A non-climatic scenario describes the socio-economic status and greenhouse gas emissions on Earth (IPCC-TGCIA 1999). There have been three such scenarios published, namely the IS92 (FAR, SAR 1992), SRES (TAR, AR4, 1998, 2007), and the representative concentration pathways (RCPs) (AR5, 2013). This study considers RCP2.6, RCP4.5, and RCP8.5. The RCP2.6 scenario predicts a maximum radiative forcing of 3 W/m^2 by 2050, followed by a decreasing trend. According to scenario RCP4.5, radiative forcing will increase until 2070 before stabilizing. Under the RCP8.5 scenario, radiative forcing will increase until the end of the 21st century when it will reach 8.5 W/m^2. In terms of CO_2 concentration the RCP2.6 and RCP8.5 forecast the smallest and largest concentrations by 2100, respectively (van Vuuren et al., 2011).

2.4. Downscaling

The process of generating regional (local) climate change scenarios from AOGCM to increase the resolution of the models in terms of temporal and spatial is called downscaling (Wilby and Harris, 2006). This work considers three downscaling methods: Change Factor (Delta), the ClimGEN model, the LARS-WG model, and GP, which are described next.

(a) Change factor method (Delta)

This work calculates the values of the difference between the simulated average temperature (and relative humidity) in the month i corresponding to the future period and the simulated average precipitation corresponding to baseline period [Equation (1)], and the values of the ratios of the simulated average precipitation (and wind speed, solar radiation on the earth's surface) in the month i corresponding to the future period over the simulated average precipitation (and wind speed, solar radiation) corresponding to the baseline period [Equation (2)] in each cell of the computational network:

$$\Delta X_i = \overline{X}_{AOGCM,fut,i} - \overline{X}_{AOGCM,base,i} \tag{1}$$

$$\Delta Y_i = \overline{Y}_{AOGCM,fut,i} \div \overline{Y}_{AOGCM,base,i} \tag{2}$$

in which ΔX_i = the climate-change scenario for the difference in

average temperature and relative humidity in month i, andΔY_i = the climate-change scenario for the ratios of precipitation, solar radiation, relative humidity, and wind speed in a month i; $\overline{X}_{AOGCM,fut,i}$ = the average temperature (and relative humidity) in a month i simulated by the AOGCMs corresponding to the future period, $\overline{X}_{AOGCM,base,i}$ = the average temperature (and relative humidity) in month i simulated by the AOGCMs corresponding to the baseline period; $\overline{Y}_{AOGCM,fut,i}$= the average precipitation (wind speed, solar radiation) in a month i simulated by the AOGCMs corresponding to the future period, $\overline{Y}_{AOGCM,base,i}$= the average precipitation (wind speed, solar radiation) in a month i simulated by the AOGCMs corresponding to the baseline period.

The calculated differences (equation (1)) are added to the observed monthly averages of the relevant variable (surface air temperature, and relative humidity) [Equation (3)], and the ratio values (equation (2)) are multiplied by the observed values (precipitation, wind speed, or radiation) [Equation (4)] (Wilby and Harris, 2006):

$$X_i = X_{obs,i} + \Delta X_i \tag{3}$$

$$Y_i = Y_{obs,i} \bullet \Delta Y_i \tag{4}$$

in which $X_{obs,i}$ and $Y_{obs,i}$ = the time series of observed temperature and precipitation in the baseline period, respectively, X_i and Y_i = the time series projected by the climate scenarios for temperature (relative humidity) and precipitation (wind speed, solar radiation) corresponding to month i in future periods.

(b) The ClimGEN model

The ClimGEN model is a weather generator that was developed by Campbell (1990). ClimGen generates precipitation, daily maximum and minimum temperature, solar radiation, air humidity, and wind speed. The ClimGEN model (Stöckle et al., 1999) is a modified version of the WGEN model (Richardson and Wright, 1984). The ClimGEN algorithm starts with precipitation simulation. The generation of precipitation is based on two assumptions. (1) the rainfall status on day t is related to the rain status on day/t, and (2) the amount of rainfall on rainy days is described by a suitable probability distribution function. The first assumption describes a type of model called a Markov chain. The result of Markov modeling of rainfall status (occurrence or non-occurrence) in the transition probability matrix is summarized in Equation (5):

$$P = \begin{bmatrix} P_{t-1,t} \end{bmatrix} = \begin{bmatrix} P_{dd} & P_{dw} \\ P_{wd} & P_{ww} \end{bmatrix}, \begin{cases} P_{dd} = 1 - P_{dw} \\ P_{wd} = 1 - P_{ww} \end{cases} \tag{5}$$

in which $P_{t-1,t}$ = the probability of transition from one state on day/t to another state on day t; and indexes d and w = determines whether a particular day is dry or wet.

The rainfall status on day t is determined by applying computer algorithms based on the congruential method (McCuen, 2002) and generating a random number (u_t) in the range (0,1). The generated random number is compared with one of the transition probabilities P_{dw} or P_{ww} (depending on whether the day/t is dry or wet).

If $u_t < P_{dw}$ or $u_t < P_{ww}$, then day t is set to be dry, otherwise it is set to wet. Concerning assumption (2) it has been determined that in many parts of the world the Weibull distribution has a good fit on the daily rainfall values. The Weibull cumulative distribution function is defined by Equation (6):

$$F_R(r) = 1 - exp\left[-\left(\frac{r}{\beta}\right)^{\alpha} \right] \tag{6}$$

in which $F_R(r)$ = the cumulative probability of precipitation equal or less than r; and α and β = parameters of the distribution function that are calculated for monthly precipitation. This distribution is sampled to each precipitation event using the inverse method according to Equation (7):

$$r = \beta \left(ln\frac{1}{1 - F_R} \right)^{\frac{1}{\alpha}} \tag{7}$$

Unlike rainfall, which is simulated independently, modeling of other weather variables such as maximum temperature (T_x), minimum temperature (T_n), and solar radiation (R_s) are affected by rainfall conditions on the desired day. The ClimGEN model uses the Richardson (1981) method to generate minimum and maximum temperature data. The latter method assumes weakly stationary (second-order stationarity) data, and the variables T_x and T_n are expressed as a first-order multivariate auto-regressive model according to Equation (8):

$$Z_t(j) = AZ_{t-1}(j) + B\varepsilon_t(j) \tag{8}$$

in which $Z_t(j)$ = the 3×1 matrices for day t whose elements are the residuals of T_x (for $j = 1$) and T_n (for $j = 2$), ε_t = the 3×1 matrix of independent random components normally distributed with mean zero and with variance σ^2. A and B = 3×3 matrices whose elements are defined as equation coefficients. After calculating Z_t, the daily values of T_x and T_n are estimated from Equation (9):

$$X_t(j) = Z_t(j)S_t(j) + \overline{X}_t(j) \tag{9}$$

in which $X_t(j)$ = the daily values of T_x (for $j = 1$) and T_n (for $j = 2$); $S_t(j)$ and $\overline{X}_t(j)$ = standard deviation and mean of variable j for day t, respectively.

The values $\overline{X}_t(j)$ and $S_t(j)$ vary depending on the wet or dry conditions of a given day. The total solar radiation simulation is also produced using the maximum and minimum temperatures and is performed using equation (10) proposed by Bristow and Campbell (1984):

$$Rs_t(j) = C[1 - \exp(-D \times \Delta T)]R_0 \tag{10}$$

in which C and D = experimental coefficients ΔT = the range of the temperature changes (difference between the maximum temperature and the minimum temperature) (in degrees Celsius), and R_0 = sunlight at the top of atmosphere (in megajoules per square meter per day).

It should be noted that all the required parameters in the ClimGEN model are determined on a monthly basis and spline functions are used for daily interpolation of the monthly parameters.

(c) The LARS-WG model

This model is a random weather data generator that is used to generate minimum and maximum temperatures, precipitation, and radiation daily under climate change conditions. This model was developed by Racsko et al. (1991) and was revised by Semenov and Barrow (1997). The LARS-WG model serves two purposes: (1) to provide a means of simulating synthetic weather time-series with statistical characteristics corresponding to the observed statistics at a site, (2) to provide a long-term average of weather time series for stations with data statistics or where it is not possible to monitor some needed variables. LARS-WG utilizes semi-empirical distributions for the lengths of wet and dry day series, daily precipitation, and daily solar radiation, according to Equation (11), which defines a histogram with ten intervals, $[a_{i-1}, a_i)$, where $a_{i-1} < a_i$, and h_i denotes the number of events from the observed data in the i-th interval.

$$Emp = \{a_0, a_i; h_i, i = 1, \cdots, 10\} \tag{11}$$

Random values from the semi-empirical distributions are chosen first by selecting one of the intervals, and then selecting a value within that interval from the uniform distribution assuming the data adheres to a uniform distribution in the desired interval. Such a distribution is flexible and can be approximated with a wide variety of shapes by adjusting the intervals $[a_{i-1}, a_i)$. The intervals $[a_{i-1}, a_i)$ are chosen based on the expected properties of the weather variables. The intervals $[a_{i-1}, a_i)$ are equally spaced for solar radiation between the minimum and maximum values of the observed data for the month. The interval size gradually increases as i increases for the lengths of dry and wet series as well as for precipitation. Based on the wet or dry state of the day, the daily mean and the daily standard deviation correspond to stochastic processes. In the LARS-WG generator, maximum and minimum temperatures are defined by the same algorithms as in ClimGEN; however, the

Table 2
GP specifications used in the present study.

Number	Type of Parameter	The value
1	Generations without improvement	150
2	Generations since start of a run	200
3	Maximum number of runs	100
4	Maximum program size	512

interpolation of monthly parameters is based on a finite Fourier series of order 3.

(d) GP

GP, developed by Koza (1992), is a leading evolutionary algorithm. GP, unlike the GA, operates on a tree structure of formulas instead of a series of binary digits, and tree structures are created from a set of functions (mathematical operators used in formulas) and terminals (problem variables and constant numbers). GP uses the objective function to compare different generated solutions of the problem being solved in a step-by-step process of correcting the data structure and finally calculating the appropriate solution (Ferreira, 2002). GP first defines the existing blocks, which include the input and target variables and their connecting function. The connecting functions between input and output variables allow GP to automatically select the appropriate variables of the model and delete the unrelated variables, which reduce the dimensions of the input variables. The appropriate structure of the model and its coefficients are determined next. Selecting the model's appropriate inputs is a key choice in GP. This becomes more significant when using secondary input data because providing unrelated input data reduces model accuracy and creates more complex models (Chen, 2003). The GP step-by-step process is as follows: (1) an initial population is generated randomly (chromosome formation); (2) Input the initial population (chromosomes) and evaluate each individual (gene) of the population using fitness functions (identifying the most influential individuals in a population); (3) selection of effective genes for mutation, mating and reproduction of new individuals with modified traits (offspring); (4) apply a repetitive development process to the offspring in each population. The fourth step is repeated a specified number times or until the best solution is obtained according to a user-defined termination criterion (Liong et al., 2002). This work applied GP with the Discipulus software, which is a product of Register Machine Learning Technologies Inc. The values of the parameters chosen to be used with the Discipulus software are listed in Table 2 (Franco, 2000).

2.5. Rainfall-runoff simulation

This work applied ANN, the IHACRES model, and the SWAT to perform monthly rainfall-runoff simulations.

(a) ANN model

Artificial neural networks are dynamic systems that, by processing experimental data, transfer the knowledge or patterns hidden in the data to the network structure and learn general rules based on numerical data or samples. Artificial neural networks extract patterns or regression functions hidden in large data sets and use them to predict values for a new set of information. Each artificial neural network is made up of processing elements or artificial neurons, which can be organized in different ways to form the network structure. The neuron, as the smallest data processing unit in an artificial neural network, forms the building block of an ANN. Cells are made up of a combination of several neurons, which, depending on the type of cell, have specific tasks in a network. The connections between cells belonging to different layers determine the structure of the ANN. The neural network consists of several layers (input layers, hidden layers, and output layers). Layers are responsible for receiving data, processing data, and generating output quantities (Thiery et al., 2008). The steps of a neural network model for forecasting or estimating include recognizing input and output variables, normalizing input and output values to (0,1) range, selecting the appropriate

geometry for the neural network, training with identifying data, testing the network with data independent of the training set to continue training the network and its parameters as needed (Anagu et al., 2009). This work implements an ANN to simulate runoff with the MATLAB software. The observed data was input to the ANN, training it with the data for the period 1971–1990, and the trained ANN was tested with data for the period 1991–2000, and then applied for prediction of runoff.

(b) The IHACRES model

This is a lumped conceptual model for rainfall-runoff simulation proposed by Jakeman and Hornberger (1993) to predict runoff from rainfall. The model consists of two modules, namely, a non-linear loss module and a linear unit hydrograph module. Rainfall (r_k) and temperature (t_k) in each time step k are converted into effective rainfall by the non-linear module, the effective rainfall is, in turn, converted to surface runoff in each time step by the linear unit hydrograph module.

Calculation of effective rainfall in time step k (u_k):

$$u_k = s_k * r_k \tag{12}$$

where s_k = the experimental basin moisture coefficient which is a function of evapotranspiration in the basin and is expressed by Equation (13):

$$s_k = C * r_k + \left(1 + \frac{1}{\tau_w(t_k)}\right)^{s_{k-1}} s_0 = 0 \tag{13}$$

$\tau_w(t_k)$ controls the value of the s_k index in Equation (13) when no rainfall occurs according to equation (14), R denotes the reference temperature; parameter C is determined in such a way that the effective rainfall volume and the observed runoff are equal in the calibration period;

$$\tau_w(t_k) = \tau_w e^{0.062f(R-t_k)} \tau_w(t_k) \rangle 1 \tag{14}$$

where τ_w and f denote the basin drying time constant and a temperature adjustment coefficient, respectively.

Runoff is predicted in time step k (x_k) with equation (15):

$$x_k = a^{(q)} x_{k-1} + b^{(q)} u_{k-1} + a^{(s)} x_{k-1} + b^{(s)} u_{k-1} \tag{15}$$

in which q and s denote respectively the separation of the basin hydrograph into a fast hydrograph *(q)* and slow hydrograph *(s)*. The IHACRES model involves three parameters namely, τ_w, f, and C from the non-linear module (Equations (12), (13) and (14)), and four parameters, namely $a^{(q)}$, $a^{(s)}$, $b^{(q)}$, and $b^{(s)}$ from the linear unit hydrograph module [Equation (15)] that must be calibrated based on observed data.

(c) SWAT

The SWAT is a continuous, conceptual, and distributed model that uses the water balance equation to simulate hydrological processes in a basin according to Equation (16):

$$\Delta sw = \sum_{i=1}^{t} \left(R_{day} - Q_{surf} - E_a - W_{seep} - Q_{gw}\right) \tag{16}$$

in which Δsw = changes of water stored in the soil; R_{day} = rainfall; Q_{surf} = surface runoff; E_a = actual evapotranspiration; W_{seep} = water infiltrated into the unsaturated soil zone; and Q_{gw} = groundwater flow (which joins the river). All the variables are in millimeters and on a daily time scale (Mengistu, 2009).

SWAT provides two surface runoff computation methods: the soil conservation service (SCS) modified method and the Green and Ampt infiltration method (Green and Ampt, 1911). The SCS method calculates the runoff depth based on the curve number, water infiltration into the soil, and initial soil moisture. The calculation of the runoff depth is as follows:

$$Q_{surface} = \frac{\left(R_{day} - I_a\right)^2}{\left(R_{day} - I_a + S\right)} \tag{17}$$

in which $Q_{surface}$ = the accumulated runoff (mm); R_{day} = the rainfall depth for the day (mm); I_a = initial abstraction (mm) and s = the potential maximum moisture retention after runoff begins (mm). To remove the necessity for independent estimation of initial abstraction a linear function between I_a and s was introduced by the SCS: $I_a = \lambda S$, where λ is an initial abstraction ratio. λ ranges between 0 and 0.3. The variable S varies with antecedent soil moisture and other variables, and it is calculated as follows:

$$S = 25.4 \left(\frac{1000}{CN} - 10\right) \tag{18}$$

in which CN = curve number of water penetration into the soil (Mengistu, 2009).

A watershed is divided into a number of sub-watersheds based upon drainage areas of the tributaries, and each sub-watershed is further divided into a number of hydrologic response units (HRU) based on land use and land cover, soil and slope characteristics. Soil water, surface runoff, sediment and chemical elements are calculated first for each HRU, and then for each sub-watershed, and finally for the entire watershed (Hosseini, 2014).

Particle swarm optimization (PSO) and the SUFI2 algorithm are applied in this work to calibrate the SWAT parameters. PSO and the SUFI2 algorithm are described next.

(i) Particle Swarm Optimization (PSO)

The basis of PSO is the simulation of the movement of the members or particles of a group of animals, such as birds or fishes (Kennedy and Eberhart, 1995). PSO, like other evolutionary computational algorithms, generates a population of potential solutions to a problem for exploring the search space. PSO assigns to each member of the population of solutions an adaptive speed (relocation) and a memory. Thus, the particles remember the best position they can find in the search space. Therefore, each particle moves in two directions: (i) towards the best situation they have ever occupied; (ii) towards the best situation that the best member in their neighborhood has ever occupied.

Assume that the search space for problem is D dimensional, so that the ith particle of the population can be represented by D-dimensional vector $X_i = (x_{i1}, x_{ii}, ..., x_{iD})^T$ and a velocity vector $V_i = (v_{i1}, v_{ii}, ..., v_{iD})^T$. The best position occupied by each particle is denoted by *pbest,* and the best position occupied by anyone in the population is denoted by *gbest*. The population moves according to Equations (19) and (20):

$$v_{i,d}^{n+1} = W v_{i,d}^n + c_1 r_1^n \left(pbest_{i,d}^n - x_{i,d}^n\right) + c_2 r_2^n \left(gbest_d^n - x_{i,d}^n\right) \tag{19}$$

$$X x_{i,d}^{n+1} = x_{i,d}^n + v_{i,d}^{n+1} \tag{20}$$

in which $d = 1, 2, ..., D$, $i = 1, 2, ..., N$, N = population size; W = inertia weight constant; c_1 and c_2 = two constants and positive coefficients, which are called cognitive and social parameters, respectively; r_1 and r_2 = random numbers in the range [01] with uniform distribution; $n = 1,2, ..., n^*$ = index for the algorithmic iterations. The particles' maximum velocity is denoted by W_{max}. The value of W_{max} is central to the optimization search because high values of W_{max} may cause high particle dispersion thus preventing some particles of finding suitable solutions. On the other hand, low values of W_{max} may prevent proper search of the search space. The parameter W in Equation (19) is used to control the effect of previous speeds on current speeds. This parameter is important for balancing the global search, also known as exploration (when W takes relatively high values), and the local search, known as exploitation (when W takes relatively low values). Experimental results have shown that it is best to first assign a relatively large value to W to improve the overall exploration of the search space, and gradually reduce its value to improve the solution extraction (Shi and Eberhart, 1998; Shi and Eberhart, 1999). Equation (21) is used assign the value of W:

$$W = W_{max} - \frac{(W_{max} - W_{min})*n}{iTer_{max}} \tag{21}$$

in which W_{max} = the first inertia weight; W_{min} = the final inertia weight; $iTer_{max}$= maximum number of iterations; and n = the iteration number. Experimental studies indicate that the value of W should be less than 1 and according to its best value is between 0.4 and 0.9.

The coefficients c_1 and c_2 do not have a significant effect on convergence, although appropriate values may result in increased convergence speed and improved local solution. A study of c_1 and c_2 was conducted by Kennedy (1998), from which it was recommended that $c_1 = c_2 = 2$, but other experimental results indicate that that $c_1 = c_2 = 0.5$ may produce better results. More research suggests that selecting c_1 larger than c_2 (with $c_1 + c_2 \leq 4$), may lead to better results (Carlisle and Dozier, 2001).

(ii) The SUFI2 algorithm from Swat-cup

Inverse modeling (IM) algorithms have become a common for model calibration. The SUFI2 algorithm is of the IM variety. It receives the values of the observed data and the allowable ranges of the SWAT parameters (such as the soil curve number, snowmelt temperature, and others) and it estimates the optimal parameter values (Abbaspour et al., 2007). The objective function of the SUFI2 algorithm must be defined in the first step. Several studies have shown that the SUFI2 results vary with the choice of different objective functions (Sao et al., 2020). The second step defines the upper and lower limits of each parameter. It is assumed that the parameters are evenly distributed across their ranges. Equation (22) represents the range of the j-th parameter b_j.

$$b_j : \left[b_{j,abs-Min} \leq b_j \leq b_{j,abs-Max}\right] j = 1, \cdots, m \tag{22}$$

In which $b_{j,abs-Min}$ and $b_{j,abs-Max}$ denote the lower and the upper bounds of the range of the j-th parameter (b_j). The range in equation (22) must be selected as large as possible while being physically meaningful (Dillaha and Beasley 1983).

The third step involves the parameters' sensitivities. Sensitivity evaluation is performed by changing one parameter in each step while keeping all other parameters constant, to assess the effect of changes in each parameter on the objective function. The fourth step evaluates the range of uncertainty of each parameter by means of Latin Hypercube (LH) Sampling.

$$b_j : \left[b_{min} \leqslant b_j \leqslant b_{max}\right], j = 1, \cdots, m \tag{23}$$

in which b_{min} b_{min} and b_{max} b_{max} denote respectively the lower and the upper bounds of the initial uncertainty ranges of the j-th parameter (b_j b_j). In general, the above ranges are smaller than the absolute ranges they are subjective, and are dependent upon experience.

The fifth step implements sampling with LH in each simulation step. LH sampling divides the probability distribution of a random variable into N^* intervals. Each of the intervals has the same probability and is equal to $\frac{1}{N^*}$. These intervals are ranked randomly. A value of each variable is then randomly extracted from each of these intervals (Dillaha and Beasley, 1983). The sixth step calculates objective function selected in the first step in each simulation step. The seventh step calculates the elements $J_{i,j}$ of the sensitivity matrix for the objective function using Equation (24):

$$J_{i,j} = \frac{\Delta g_i}{\Delta b_j} i = 1, \cdots, c_2^n j = 1, \cdots, m \tag{24}$$

in which c_2^n = the number of rows in the matrix, which is equal to the number of simulation steps, j = index for the matrix columns, whose number is equal to the number of parameters, g = objective function, b_j =desired parameter, Δg_i=objective function change, $\Delta b_j \Delta b_j$=desired parameter change. The eighth step calculates the 95 % confidence interval (95PPU) for all parameters by means of the 2.5th (X_L) and 97.5th (X_U) percentiles. The average distance between the upper and lower 95 PPU limits ($\overline{d_X}$) is obtained from Equation (25) (Abbaspour 2007):

$$\overline{d_X} = \frac{1}{M}\sum_{i=1}^{M}(X_U - X_L)_i \tag{25}$$

in which M = The number of observed values.

The optimal state is when 100 % of the observed values are in the 95PPU confidence range and the value of $\overline{d_X}$ is close to zero. But due to measurement errors and model uncertainty a suitable value might not be obtained. Therefore, based on experience, a suitable way for estimating $\overline{d_X}$ is the calculation of the *Rfactor* according to Equation (26) (Abbaspour et al., 2007).

$$Rfactor = \frac{\overline{d_X}}{\sigma_X} \tag{26}$$

in which σ_X = The standard deviation of the measured variable X.

The ninth step adjusts the ranges of the parameters because their uncertainty is initially large. A new range for each parameter is obtained from Equations (27) and (28) (Abbaspour et al., 2007):

$$b'_{j,min} = b_{j,lower} - Max\left(\frac{(b_{j,lower} - b_{j,min})}{2}, \frac{(b_{j,max} - b_{j,upper})}{2}\right) \tag{27}$$

$$b'_{j,lower} = b_{j,upper} + Max\left(\frac{(b_{j,lower} - b_{j,min})}{2}, \frac{(b_{j,max} - b_{j,upper})}{2}\right) \tag{28}$$

where $b'_{j,min}$ and $b'_{j,max}$ denote the updated values of the minimum and maximum j-th parameter, respectively. The best p solutions are used to calculate $b_{j,lower}$ $b_{j,lower}$ and $b_{j,upper}$ $b_{j,upper}$.

This work employs the Nash-Sutcliffe efficiency (*NSE*) index [Equation (28)] as the objective function for optimizing the SWAT parameters (McCuen et al., 2006):

$$NSE = 1 - \frac{\sum_{i=1}^{M}(Q_{m,i} - Q_{s,i})^2}{\sum_{i=1}^{M}(Q_{m,i} - \overline{Q_m})^2} \tag{28}$$

in which $\overline{Q_m}$ = the average observed flow in cubic meters per second; $Q_{m,i}$ and $Q_{s,i}$ = the observed and simulated discharge values, respectively, during the simulation period; and i = the index for the data values. The value of *NSE* shows the degree of agreement between the observed and the simulated flows, and its ranges from $-\infty$ to 1, with 1 indicates perfect goodness of fit.

It is noteworthy that in the baseline period (1971–19000) the performances of downscaling methods and hydrological models were compared based on the correlation coefficient (R^2), the root mean square (*RMSE*), the maximum absolute error (*MAE*), and the NSE, [Equations (29)-(31)] (Chicco et al., 2021).

correlation coefficient (R^2)

$$R^2 = \left[\frac{\frac{1}{n}\sum_i(Q_{m,i} - \overline{Q_m})(Q_{s,i} - \overline{Q_s})}{\sigma_m \times \sigma_s}\right]^2 \tag{29}$$

where σ_m and σ_s denote the standard deviation of the measured and simulated variables. The R^2 varies between -1 and 1. It measures the degree of linear statistical association beween the measured and simulated variables. It is sometimes expressed as a percentage (see Results).

Root mean square error (RMSE)

$$RMSE = \sqrt{\frac{1}{m}\sum_i(Q_{m,i} - Q_{s,i})^2} \tag{30}$$

It takes non-negative values.

Mean absolute error (*MAE*)

$$MAE = \frac{1}{m}\sum_i|Q_{m,i} - Q_{s,i}| \tag{31}$$

Table 3
Accuracy assessment of the AOGCMs with performance criteria for rainfall.

Models	Rainfall			
	R^2 (%)	RMSE (mm)	MAE (mm)	NSE
BCC-CSM1.1	11.7	41.7	33.5	−0.7
BCC-CSM1.1(m)	22.1	37.1	29.5	−0.3
BNU-ESM	45.7	46.3	36.1	−1.1
CanESM2	25.3	45.6	35.2	−1.0
CCSM4	35.1	36.3	30.6	−0.3
CESM1(CAM5)	36.1	41.8	33.4	−0.7
CNRM-CM5	**86.1**	**12.3**	**10.7**	**0.9**
GFDL-CM3	66.5	32.8	25.8	0.0
GFDL-ESM2G	36.8	37.0	29.8	−0.3
GISS-E2-H	68.4	26.9	19.1	0.3
GISS-E2-R	38.3	27.6	21.8	0.3
MIROC5	56.8	30.0	24.8	0.1
MIROC-ESM	71.9	37.3	29.3	−0.4
MIROC-ESM-CHEM	74.6	37.6	29.2	−0.4
MPI-ESM-LR	61.3	44.8	34.7	−1.0
MPI-ESM-MR	52.9	44.1	33.8	−0.9
NorESM1-M	30.4	44.8	35.2	−1.0

Table 4
Accuracy assessment of the AOGCMs with performance criteria for average temperature.

Models	Average temperature			
	R^2 (%)	RMSE (℃)	MAE (℃)	NSE
BCC-CSM1.1	48.8	9.8	8.2	−0.3
BCC-CSM1.1(m)	48.4	9.1	7.7	−0.2
BNU-ESM	50.5	12.1	9.9	−1.0
CanESM2	45.2	14.6	12.2	−2.0
CCSM4	50.9	11.6	9.4	−0.9
CESM1(CAM5)	47.3	12.3	10.1	−1.1
CNRM-CM5	**95.1**	**3.0**	**2.7**	**0.9**
GFDL-CM3	54.8	9.7	8.0	−0.3
GFDL-ESM2G	50.6	9.8	8.2	−0.4
GISS-E2-H	92.0	11.2	10.9	−0.8
GISS-E2-R	93.6	11.1	10.9	−0.7
MIROC5	55.1	9.4	7.7	−0.2
MIROC-ESM	92.5	8.9	8.4	−0.1
MIROC-ESM-CHEM	91.9	8.7	8.2	−0.1
MPI-ESM-LR	92.1	12.2	11.9	−1.1
MPI-ESM-MR	92.8	12.0	11.7	−1.0
NorESM1-M	45.2	13.0	10.6	−1.4

Table 5
Accuracy assessment of the AOGCMs with performance criteria for maximum temperature.

Models	Maximum temperature			
	R^2 (%)	RMSE (℃)	MAE (℃)	NSE
BCC-CSM1.1	37.3	10.4	9.3	0.2
BCC-CSM1.1(m)	37.7	10.4	9.3	0.2
BNU-ESM	40.5	11.0	9.6	0.1
CanESM2	35.9	16.7	14.3	−1.1
CCSM4	41.3	10.9	9.5	0.1
CESM1(CAM5)	39.9	11.1	9.7	0.1
CNRM-CM5	91.0	5.2	4.6	0.8
GFDL-CM3	**90.5**	**4.2**	**3.7**	**0.9**
GFDL-ESM2G	86.4	4.8	4.1	0.8
GISS-E2-H	84.4	9.0	8.3	0.4
GISS-E2-R	85.9	8.8	8.1	0.4
MIROC5	46.0	10.1	8.8	0.2
MIROC-ESM	86.2	7.8	7.2	0.5
MIROC-ESM-CHEM	85.3	7.7	7.0	0.6
MPI-ESM-LR	87.1	9.6	9.0	0.3
MPI-ESM-MR	87.6	9.3	8.8	0.3
NorESM1-M	36.3	12.0	10.6	−0.1

Table 6
Accuracy assessment of the AOGCMs with performance criteria for minimum temperature.

Models	Minimum temperature			
	R^2 (%)	RMSE (℃)	MAE (℃)	NSE
BCC-CSM1.1	54.5	10.8	9.1	−1.5
BCC-CSM1.1(m)	54.9	9.5	7.5	−0.9
BNU-ESM	53.1	14.2	12.2	−3.4
CanESM2	50.3	13.0	10.9	−2.6
CCSM4	55.4	13.4	11.9	−2.9
CESM1(CAM5)	49.0	14.3	12.5	−3.4
CNRM-CM5	**94.3**	**2.0**	**1.6**	**0.9**
GFDL-CM3	53.9	11.0	9.0	−1.6
GFDL-ESM2G	93.1	11.1	10.6	−1.6
GISS-E2-H	93.0	13.8	13.6	−3.1
GISS-E2-R	95.2	13.8	13.6	−3.1
MIROC5	58.2	9.4	7.7	−0.9
MIROC-ESM	93.7	10.4	10.1	−1.4
MIROC-ESM-CHEM	92.2	8.8	8.5	−0.7
MPI-ESM-LR	91.2	14.9	14.6	−3.8
MPI-ESM-MR	91.9	14.8	14.5	−3.7
NorESM1-M	47.7	14.4	12.8	−3.5

Table 7
Accuracy assessment of the downscaling models with performance criteria.

Climatic variable	Performance criteria	Downscaling model			
		Change Factor	LARS-WG	ClimGen	GP
Rainfall	R^2 (%)	23.99	61.21	26.52	27.41
	RMSE (mm)	51.46	29.02	43.43	38.39
	MAE (mm)	33.86	18.01	27.68	29.89
	NSE	−0.43	0.54	−0.02	0.26
Maximum Temperature	R^2 (%)	93.47	96.47	90.66	91.76
	RMSE (℃)	2.88	2.88	6.51	3.23
	MAE (℃)	2.19	2.19	5.62	2.64
	NSE	0.92	0.92	0.6	0.9
Minimum Temperature	R^2 (%)	42.92	86.48	62.56	86.07
	RMSE (℃)	7.62	2.8	4.56	3.93
	MAE (℃)	3.49	2.99	3.72	3.93
	NSE	−0.25	0.69	0.55	0.86

MAE is most useful if outliers are present in the data. It takes non-negative values.

3. Results and discussion

3.1. Performance assessment of the AOGCMs and choosing the best model

The best performance among 17 AOGCMs was selected with the R^2, *RMSE*, *MAE* and *NSE* criteria calculated for the baseline period (1971–2000). Tables 3-6 detail the results for rainfall, average temperature, maximum temperature, and minimum temperature. An accurate model is best characterized by a high correlation coefficient (R^2) and a low mean absolute error. The CNRM-CM5 model performed better than other models with in terms of rainfall, average temperature, and minimum temperature. The GFDL-CM3 model performed better than other models for maximum temperature.

3.2. Calculation of climate change scenarios in future periods

The climate-change scenarios for temperature and rainfall in the basin were calculated for the future period after choosing the best models for projecting climatic variables under the RCP2.6, RCP4.5 and RCP8.5 scenarios. The time series of temperature and rainfall projections were downscaled to the basin scale. The downscaling methods that were implemented were Change Factor, LARS-WG, ClimGen, and GP. The results of the calibration for the downscaling models are listed in Table 7. It is noteworthy that the LARS-WG and ClimGen methods
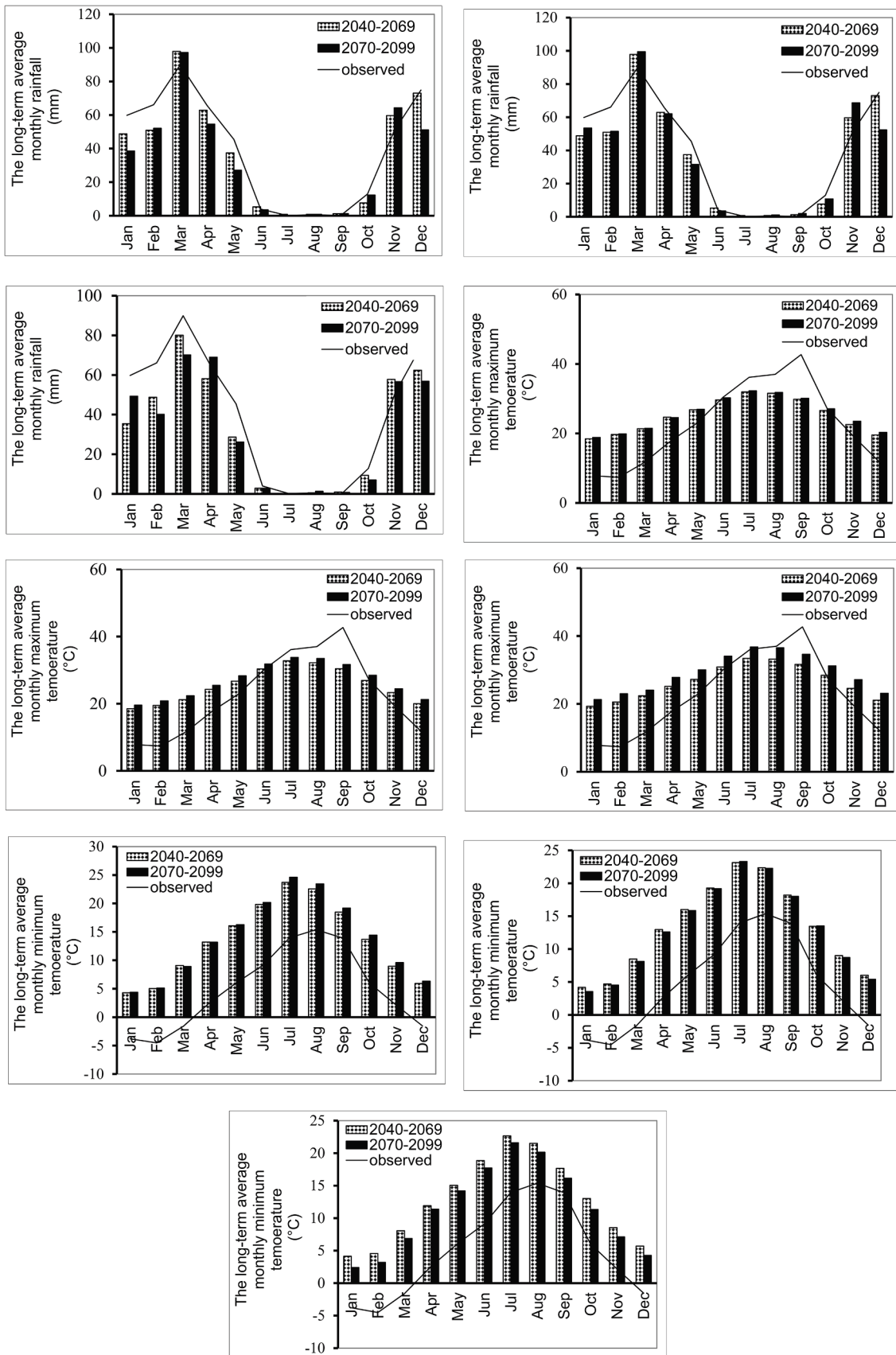
Fig. 2. Monthly long-term rainfall in 2040–2069 and 2070–2099 under (a) RCP2.6, (b) RCP4.5, and (c) RCP8.5; Monthly long-term maximum temperature in 2040–2069 and 2070–2099 under (d) RCP2.6, (e) RCP4.5 and (f) RCP8.5; Monthly long-term minimum temperature in 2040–2069 and 2070–2099 under (g) RCP2.6, (h) RCP4.5 and (i) RCP8.5.

Table 8

Calibration parameters of the IHACRES model.

Linear hydrograph module		Non-linear loss module		
$a^{(s)}$	$b^{(s)}$	F	t_w	C
−0.495	0.505	4.3	5.8	0.001151

Table 9

Performance criteria for IHACRES, ANN, and the SWAT.

Model	Time period	R^2 (%)	RMSE (m^3/s)	MAE (m^3/s)	NSE
IHACRES	1971–1990 (Calibration)	71.16	4.93	2.72	0.71
	1991–2000 (Verification)	72.87	3.89	2.44	0.72
ANN	1971–1990 (Calibration)	40.85	6.99	4.11	0.41
	1991–2000 (Verification)	32.53	6.35	7.18	0.24
SWAT/SUFI2	1974–1990 (Calibration)	59.78	5.58	3.38	0.55
	1992–2000 (Verification)	60.75	6.60	3.63	0.25
SWAT/PSO	1974–1990 (Calibration)	54.44	6.25	4.61	0.43
	1992–2000 (Verification)	63.83	7.26	6.12	0.09

predicted well the minimum and maximum temperatures but not the average temperature. Therefore, the methods were compared based on rainfall, maximum temperature, and minimum temperature. Table 7 indicates the Change Factor and ClimGen methods do not perform well in predicting rainfall and minimum temperature in 1971–2000, while LARS-WG and GP predict rainfall, maximum temperature, and minimum temperature better than other methods. In general, the LARS-WG model performed better than the other three methods.

The LARS-WG method was chosen to estimate rainfall, maximum, and minimum temperature in the future periods (2040–2069) and (2070–2099) due to its superior performance. The corresponding results are presented in Fig. 2. Fig. 2(a)-(c) shows that the rainfall corresponding to the RCP2.6 and RCP4.5 scenarios in the two future periods would decrease in all months except March and November. It is also shown that the rainfall in the period 2070–2099 would be less than that for the period 2040–2069, except for February, October, and November. Also, rainfall in the period 2070–2099 would be higher than it was in the period 2040–2069, except for October and December. According to the RCP8.5 scenario, precipitation will be reduced in all months except April and November. With regard to future periods, more rain would fall in January and April than it would in the near future, but less rain would fall in all other months in 2070–2099 than in 2040–2069. Fig. 2(d)-(f) illustrates that, according to scenarios RCP2.6, RCP4.5, and RCP8.5, the maximum temperature for 2040–2069 and 2070–2099 is projected to increase. By comparing future periods, it appears that temperatures will increase more in 2070–2099 than in 2040–2069. The comparison of seasonal projections under the three emissions scenarios establishes that winter and summer would have the highest and lowest increases in temperature, respectively, compared to the observed values in the future two periods. It is seen in Fig. 2(g)-(i) that under the three emissions scenarios the minimum temperature would increase in the future two periods compared to the baseline period. The comparison of future periods establishes that under the RCP2.6 scenario the minimum temperature would increase in 2070–2099 from late spring to late summer, but in spring and early summer, the minimum temperature would be higher in 2040–2069 than in 2070–2099. Under the RCP4.5 and RCP8.5 emission scenarios, the minimum temperature in the period 2070–2099 would be lower than in 2040–2069 in all months.

3.3. Calibration and testing results for the rainfall-runoff models

(a) The IHACRES model

The IHACRES model was calibrated and tested with the average monthly rainfall and temperature data. Observed temperature, precipitation, and runoff for 1971–2000 were input information to IHACRES.

IHACRES was calibrated for the first 20 years of the period (1971–1990) and tested for the second 10 years of the period (1991–2000). Table 8 outlines the parameters calibrated in the model, while Table 9 summarizes the results related to the calibration and testing of IHACRES. For the calibration and testing periods, Fig. 3(a)-(b) show the time series of river flow. According to Table 9 and Fig. 3(a)-(b) the R^2 in the calibration and verification periods was high, the error rates were low, and the *NSE* is close to one. This provides ample evidence that the IHACRES has good predictive skill for river flow simulation in the study area.

(b) The ANN model

ANN was run in MATLAB with two hidden layers, each of which has two neurons, the transmission function is tansig, and the training was performed with the Levenberg-Marquardt algorithm. The results of ANN training and testing are listed in Table 9, and the river flow time series for the calibration and testing periods are depicted in Fig. 3(c)-(d). The ANN results in Table 9 and Fig. 3(c)-(d), due to the calculated low *NSE*, it is clear that this model did not perform accurately in estimating the peak flow compared to the IHACRES. Also, according to the R^2 and the magnitude of the errors, it is determined that the accuracy of this model is lower than the IHACRES's.

(c) The SWAT

Raster maps, including digital elevation map (DEM), soil and land use of Ravansar Sanjabi basin were extracted (Fig. 4). Information about the soils and land uses in the Sanjabi Basin is found in section of supplemental information (Appendixes A and B). Three DEMs, soil, and land uses were combined followed by performing slope classification into five categories to delineate the HRUs within the study basin. The adopted slope classification includes five categories: 0–10.66, 10.66–21.33, 21.33–31.99, 31.99–42.66 and 42.66–53.33 degrees.

Thirty-three sub-basins and 260 HRUs were formed in SWAT in the Sanjabi basin. The daily rainfall and the maximum and minimum daily temperatures of stations near the basin in the 30-year period (1971–2000) were input to SWAT. The monthly data for 1971, 1972, and 1973 were input as Warm-Up, and the SWAT2012 model was implemented in ArcGIS10.2 software with a monthly time step. The initial values of some properties of the basin, such as soil chemical composition, were not available; therefore, the SWAT can calculate these values in the Warm-Up period. The map of sub-basins and rivers is displayed in Fig. 5.

SWAT calculates runoff components, sub-surface flow, groundwater storage, and other variables and exports these as text files. SWAT store this text file in a folder called TxtIntOut, which is interfaced with the SWAT-CUP software. SWAT-CUP calibrates SWAT parameters with the SUFI2 algorithm and PSO using flow data for the period 1974–1991. SWAT-CUP tests SWAT parameters for the period 1992–2000. Tables 10 and 11 list the calibration parameters and the optimal values of these parameters derived from SUFI2 and PSO, respectively.

The results of SWAT model calibration and testing with SUFI2 and PSO are listed in Tables 9, and the river flow time series for the calibration and testing periods are displayed in Fig. 3.

The calibration results for SWAT indicate better accuracy for the SUFI2 algorithm than for PSO. However, the low *NSE* obtained with SUFI2 and PSO in the testing period establishes the low performance of the SWAT model in the simulation of peak discharges in the period 1992–2000.

Comparing three hydrological models (IHACRES, ANN, and SWAT) reveals that the performance of IHACRES was the best in this application, and, therefore, the future runoff under the three scenarios RCP2.6, RCP4.5, and RCP8.5 and the two future periods 2040–2069 and 2070–2099 are estimated with this model.

3.4. Simulation of future river flow

The IHACRES model projected the monthly time series of river flow relying on future temperature and precipitation projected values that were estimated with the LARS-WG method. Fig. 6 shows a comparison of
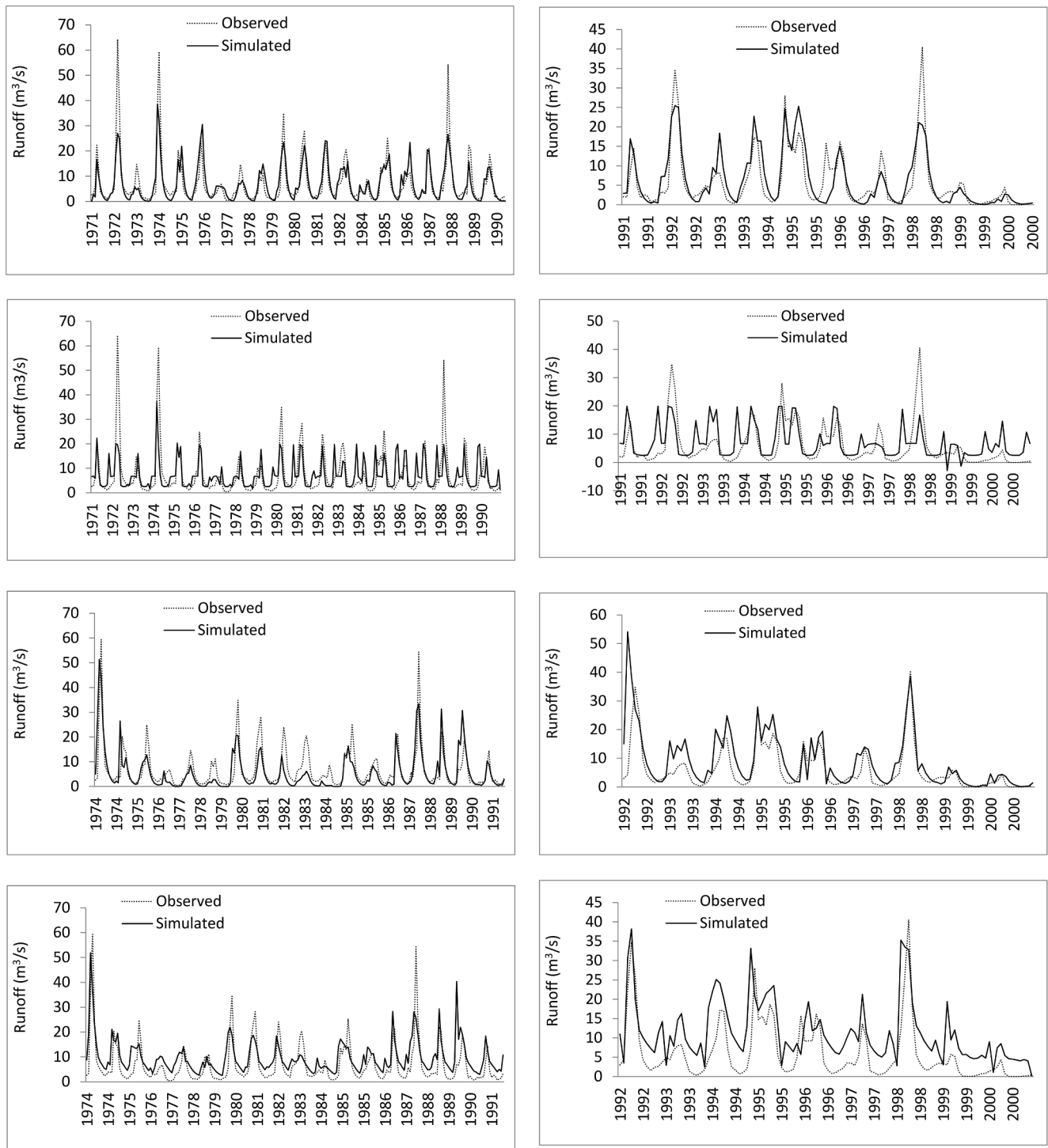
Fig. 3. Comparison of simulated and observed runoff by (a) IHACRES for calibration, and (b) IHACRES for testing, (c) ANN for calibration and (d) ANN for testing, (e) SWAT/SUFI2 for calibration and (f) SWAT/SUFI2 for testing, (g) SWAT/PSO for calibration and (h) SWAT/PSO for testing.

the average long-term monthly river flow in the 2040–2069 and 2070–2099 under the three emission scenarios RCP2.6, RCP4.5, and RCP8.5 with baseline and observed values. Also, the average long-term values of observed, baseline, and simulated runoff and future periods under different scenarios are listed in Table 12. The results are shown in Fig. 6 and Table 12 indicate that the simulated runoff values in the two future periods under the three emission scenarios in all months would decrease compared to the simulated baseline values, and the reduction from early winter until mid-summer is much larger than in the autumn. This trend is the same when comparing future runoff with observed

values. However, only in January and June under the RCP2.6 (2040–2069) and January, June, and December under RCP4.5 (2070–2099) would the future runoff be slightly larger than the observed runoff. The comparison of the emission scenarios reveals that the RCP8.5 scenario would produce a larger runoff reduction in the future than the other two scenarios, and the RCP4.5 would produce a smaller reduction in the runoff, and from the comparison of future periods it transpires that under the RCP2.6 and RCP8.5 scenarios there would be less runoff in 2070–2099 than in 2040–2069, but this trend is the opposite for RCP4.5. The annual changes in simulation runoff
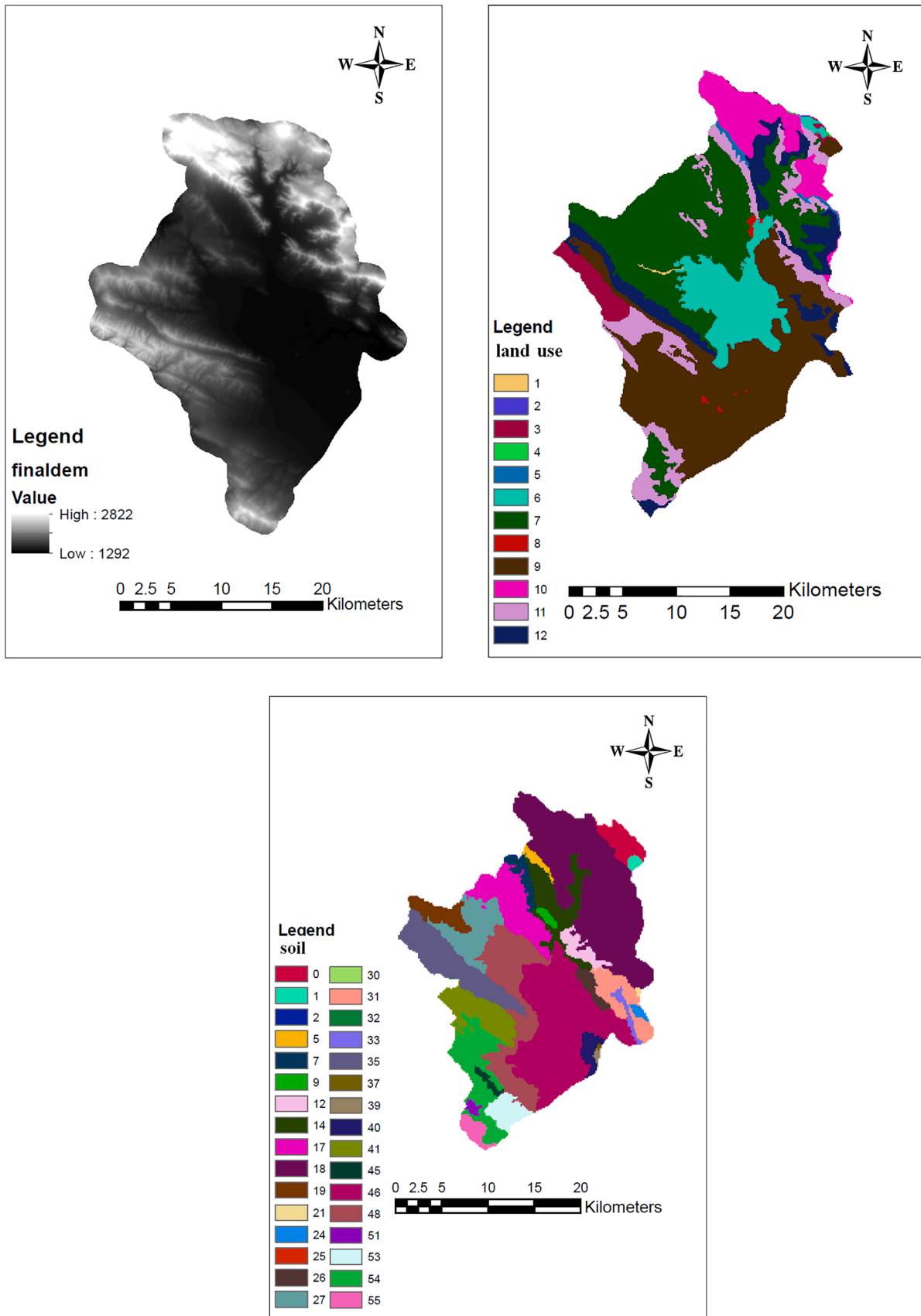
Fig. 4. (a) Digital elevation, (b) land use and (c) soil maps of the Sanjabi basin (See section of supplemental information - Appendixes A and B).
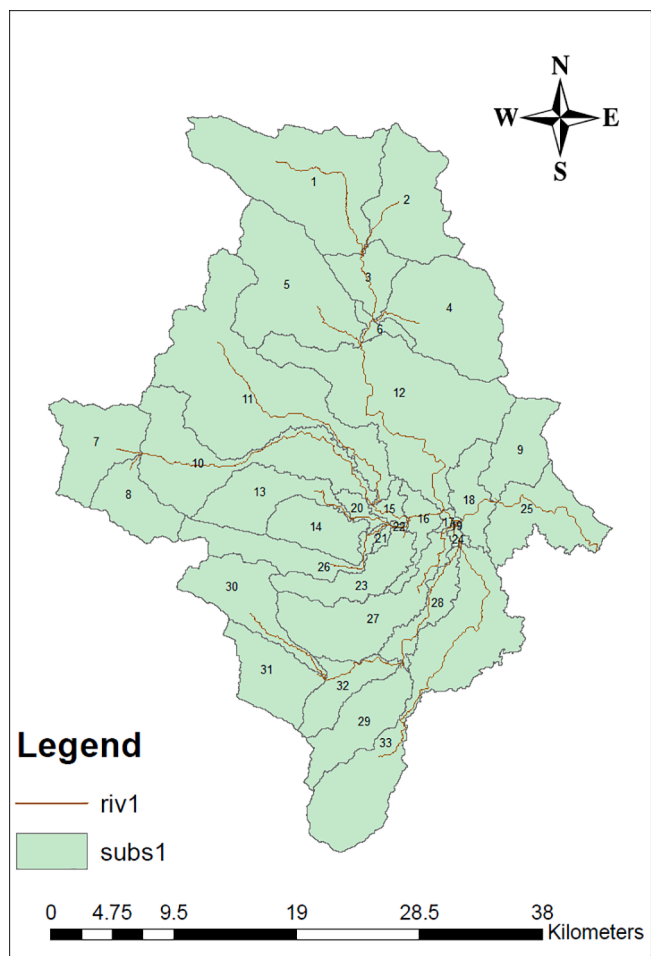
Fig. 5. Sub-basins and rivers in the Sanjabi basin.

the RCP4.5 emissions scenario for 2040–2069 and 2070–2099 would be reduced with respect to the observed values by 32.9 % and 25.6 %, respectively. The RCP8.5 shows the largest reduction of runoff, which is 42.0 and 44.3 % for 2040–2069 and 2070–2099, respectively.

4. Discussion

There is a variety of hydrology models available, so choosing the most suitable one when undertaking a study is not trivial. It is therefore necessary to conduct a comparative analysis of basin models to evaluate their capabilities and limitations in the study area. Studies comparing hydrological models provide managers and planners with strategic results to help them manage water resources. It is noteworthy that comparing the performance of several rainfall-runoff models in basins with different climates is an effective way determining which model is the most appropriate. Several hydrological models have been widely applied in recent years. The IHACRES model predicts flow better than distributed models in many cases (Littlewood and Jakeman, 1994; Ye, et al., 1997). It is also easy to implement with respect to calibration and testing. Moreover, the input data are readily available and the
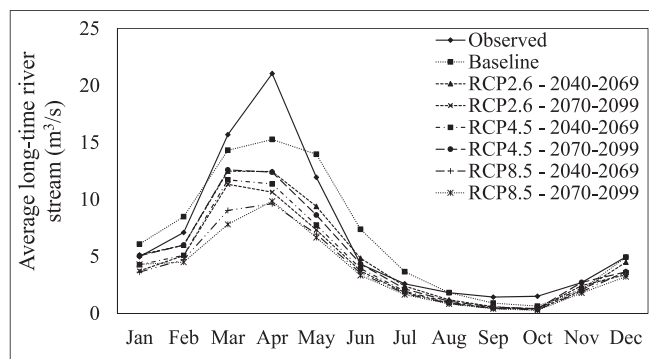

Fig. 6. Comparison of projected monthly long-term river flow (runoff) in 2040–2069 and 2070–2099 under the RCP2.6, RCP4.5, and RCP8.5 scenarios with the baseline and observed values.

calculated with the IHACRES model relative to the observed values are listed in Table 13. It is seen in Table 13 that the annual runoff reduction under the RCP2.6 emissions scenario for 2040–2069 and 2070–2099 would be 23.5 % and 36.0 %, respectively. The runoff simulated under

Table 10
SWAT parameters used in the calibration and their optimal values obtained with the SUFI2 algorithm.

Number	Parameter name	Variation range	Optimal value	Number	Parameter name	Variation range	Optimal value
1	CN2	−0.2–0.2	−0.19	9	GW_REVAP	0–0.11	0.01
2	ALPHA_BF	0.46–1	0.92	10	RCHRG_DP	0.41–1	0.82
3	GW_DELAY	30–254.11	53.14	11	SOL_BD	0.82–2.5	2.15
4	GWQMN	0.62–1.88	1.25	12	SOL_AWC	−0.2–0.16	−0.08
5	ESCO	0.19–0.73	0.46	13	SOL_K	0–0.58	0.12
6	CH_K2	14.31–104.79	59.55	14	OV_N	0.16–0.59	0.37
7	CH_N2	0.1–0.3	0.2	15	REVAPMN	0–500	0
8	ALPHA_BNK	0–0.6	0.21	16	SURLAG	8.47–25.31	16.89

Table 11
SWAT parameters used in the calibration and their optimal values obtained with PSO.

Number	Parameter name	Variation range	Optimal value	Number	Parameter name	Variation range	Optimal value
1	CN2	−0.16–0.2	0	9	GW_REVAP	0–0.17	0.01
2	ALPHA_BF	0–0.19	0.01	10	RCHRG_DP	0–1	0.82
3	GW_DELAY	30–276.16	222.82	11	SOL_BD	1.09–2.5	2.15
4	GWQMN	0–0.8	0.43	12	SOL_AWC	0–0.15	−0.08
5	ESCO	0.85–1	0.99	13	SOL_K	0–183.72	187.68
6	CH_K2	0–0.22	22.42	14	OV_N	0.01–19.26	7.24
7	CH_N2	5–42.69	0.12	15	REVAPMN	0–259.1	217.68
8	ALPHA_BNK	0–0.02	0.02	16	SURLAG	5.73–24	18.1

Table 12

The average long-term observation, baseline, and future runoff in 2040–2069 and 2070–2099 under the RCP2.6, RCP4.5 and RCP8.5 emissions scenarios.

Month	Observed	Baseline	RCP2.6		RCP4.5		RCP8.5	
			2040–2069	2070–2099	2040–2069	2070–2099	2040–2069	2070–2099
Jan	4.97	6.08	5.14	3.73	4.27	5.06	3.63	4.30
Feb	7.10	8.49	5.98	5.08	5.10	6.00	4.72	4.51
Mar	15.70	14.31	12.49	11.33	11.72	12.59	9.04	7.81
Apr	21.05	15.27	12.45	10.64	11.36	12.40	9.62	9.85
May	11.95	13.97	9.39	7.33	7.76	8.63	6.96	6.66
Jun	4.32	7.39	4.83	3.71	3.93	4.35	3.53	3.33
Jul	2.59	3.66	2.39	1.84	1.95	2.15	1.75	1.65
Aug	1.82	1.81	1.19	0.91	0.97	1.07	0.87	0.83
Sep	1.44	0.90	0.59	0.46	0.49	0.55	0.43	0.41
Oct	1.50	0.64	0.36	0.41	0.43	0.42	0.32	0.27
Nov	2.70	2.07	2.00	2.44	2.21	2.72	1.90	1.79
Dec	4.96	4.94	4.49	3.40	3.57	3.65	3.67	3.23

Table 13

The annual changes in simulation runoff relative to the observed values.

Percentage of runoff changes					
RCP2.6		RCP4.5		RCP8.5	
2040–2069	2070–2099	2040–2069	2070–2099	2040–2069	2070–2099
−23.5	−36.0	−32.9	−25.6	−42.0	−44.3

calculations are simple. Boorman and Sefton (1997) evaluated the differences between the results of two conceptual hydrologic models, and their results showed that the two models had the same capability in simulating historical flows. Despite the complexity of distributed models some researchers recommend their use because they provide more accurate predictions due to their more realistic representation of hydrologic processes and basin conditions (Ghavidelfar et al., 2011; Te Linde et al., 2008). Analysts must weigh in the tradeoffs between model complexity and ease of implementation in choosing a hydrologic model.

The impact of climate change on temperature and precipitation parameters and their influence on the hydrological cycle, forecasting, and modeling future temperature and precipitation accurately are factors that must be considered prior to engaging in future planning and choosing a hydrologic model. There have been several studies comparing the performance of models considering their accuracy for forecasting changes in weather conditions and the role that they play in simulating and predicting parameters that affect the hydrological cycle. Adamowski and Prasher (2012) evaluated SVM and ANN models to simulate rainfall in a mountain basin. His results showed the superiority of SVM. Tezel and Buyukyildiz (2016) evaluated the efficiency of ANN and SVM in estimating monthly evaporation. The latter authors reported that both models exhibited similar performance in predicting evaporation based on temperature, relative humidity, wind speed, and precipitation.

The comparison of ANN, IHACRES, and SWAT presented in this study is novel. This study was performed to determine if the use of data mining and conceptual models, where input data are readily available and calculations are relatively simple, yet they lead to better predictions than those of distributed models, whose data inputs require spatial and temporal detail. This work compared the change factor (Delta), ClimGEN, LARS-WG, and GP downscaling methods and their accuracy was measured by the R^2, *RMSE*, *MAE*, and *NSE* coefficients. Overall, the results showed that the IHACRES model performed better than the other two models, and this result was consistent with other studies that have indicated that flow simulation by the IHACRES model may be better than those produced by distributed models (Littlewood and Jakeman, 1994; Ye, et al., 1997).

5. Conclusions

This work compared the runoff projections obtained with the data-mining model (ANN), the lumped model (IHACRES), and the distributed model (SWAT) for the Sanjabi basin in Kermanshah province, Iran, under climate-change conditions. For this purpose, 17 models from the IPCC 5th assessment report climate change scenarios were adopted in this work, namely, BCC-CSM1.1, BCC-CSM1.1(m), BNU-ESM, CanESM2, CCSM4, CESM1(CAM5), CNRM-CM5, GFDL-CM3, GFDL-ESM2G, GISS-E2-H, GISS-E2-R, MIROC5, MIROC-ESM, MIROC-ESM-CHEM, MPI-ESM-LR, MPI-ESM-MR, and NorESM1-M corresponding to 2040–2069 and 2070–2099, and under three emission scenarios, i.e., RCP2.6, RCP4.5 and RCP8.5. The performance criteria R^2, *RMSE*, *MAE,* and *NSE* evaluated projections of rainfall, average temperature, and minimum temperature, and it was concluded that theCNRM-CM5 performed better than other models. The GFDL-CM3 performed better than other models with respect to maximum temperature.

The Change Factor (Delta), ClimGEN, LARS-WG, and GP methods were implemented for downscaling climate variables, and their results were evaluated with performance criteria. The LARS-WG method performed best in the Ravansar Sanjabi basin. The LARS-WG method was therefore implemented to project future rainfall and temperature. ANN, IHACRES, and SWAT were implemented to simulate runoff. These models were calibrated and their predictive skill was evaluated. Among the hydrological models the IHACRES model had the best performance with R^2, *RMSE*, *MAE* by 71.6 %, 4.93 (m^3/s), 2.72 (m^3/s) and 0.71 %, in the testing period (1971–1990), and 72.87 %, 3.89 (m^3/s), 2.44 (m^3/s) and 0.72 % in the calibration period (1992–1000). Therefore, IHACRES was applied to project future runoff. The comparison of the projected long-term average monthly runoff under the RCP2.6, RCP4.5, and RCP8.5 scenarios for 2040–2069 and 2070–2099 with baseline values reveals that the runoff would decline under all scenarios and in the two future periods. Furthermore, the annual runoff projected under the RCP2.6, RCP4.5 and RCP8.5 emissions scenarios for 2040–2069 would decline by 23.5 %, 36.0 %, and 32.9 %, respectively, in comparison to the observed runoff, and under the same scenarios for 2070–2099 the projected runoff would be reduced respectively by 25.6 %, 42.0 %, and 44.3 % compared to observed runoff.

CRediT authorship contribution statement

Seyedeh Hadis Moghadam: Methodology, Software, Validation. **Parisa-Sadat Ashofteh:** Supervision, Writing – review & editing, Conceptualization, Investigation, Validation. **Hugo A. Loáiciga:** Writing – review & editing.

Declaration of Competing Interest

The authors declare that they have no known competing financial interests or personal relationships that could have appeared to influence the work reported in this paper.

Data availability

Data will be made available on request.

References

Abbaspour, K.C., 2007. User Manual for SWAT-CUP (SWAT Calibration and Uncertainty Analysis Programs). Swiss Federal Institute of Aquatic Science and Technology, Eawag, Dübendorf, Switzerland, p. 95.

Abbaspour, K.C., Yang, J., Maximov, I., Siber, R., Bogner, K., Mieleitner, J., Zobrist, J., Srinivasan, R., 2007. Modelling of hydrology and water quality in the pre-alpine/alpine thur watershed using SWAT. J. Hydrol. 333, 413–430. https://doi.org/10.1016/j.jhydrol.2006.09.014.

Adamowski, J., Prasher, S.O., 2012. Comparison of machine learning methods for runoff forecasting in mountainous watersheds with limited data. J. Water Land Dev. 17 (1), 89–97. https://doi.org/10.2478/v10025-012-0038-4.

Afinowicz, J.D., Munster, C.L., Wilcox, B.P., 2005. Modeling effects of brush management on the rangeland water budget: Edwards Plateau, Texas. J. Am. Water Resour. Assoc. (JAWRA) 41 (1), 181–193. https://doi.org/10.1111/j.1752-1688.2005.tb03727.x.

Anagu, I., Joachim, I., Jens, U., Thilo, S., 2009. Estimation of heavy metal sorption in German soils using artificial neural network. Geoderma 152 (1–2), 104–112. https://doi.org/10.1016/j.geoderma.2009.06.004.

Ashofteh, P.-S., Bozorg-Haddad, O., Loáiciga, H.A., 2016. Development of Adaptive Strategies for Irrigation Water Demand Management under Climate Change. J. Irrig. Drain. Eng. 143 (2) https://doi.org/10.1061/(ASCE)IR.1943-4774.0001123.

Aytek, A., Kisi, O., 2008. A genetic programming approach to suspended sediment modeling. J. Hydrol. 351 (3–4), 288–298. https://doi.org/10.1016/j.jhydrol.2007.12.005.

Boorman, D.B., Sefton, C.E.M., 1997. Recognizing the uncertainty in the quantification of the effects of climate change on hydrological response. Clim. Change 35 (4), 415–434. https://doi.org/10.1023/A:1005372407881.

Bristow, K.L., Campbell, G.S., 1984. On the relationship between incoming solar radiation and daily maximum and minimum temperature. Agric. For. Meteorol. 31 (2), 159–166. https://doi.org/10.1016/0168-1923(84)90017-0.

Campbell, G.S. (1990). CLIMGEN, A program that generates weather data (precipitation, maximum and minimum temperatures). Biological Systems Engineering Dept., Washington State University, Pullman, Washington, USA.

Carlisle A. and Dozier G. (2001). "An Off-The- Shelf PSO", Proceedings of the Workshop on Particle Swarm Optimization, 1-6.

Chen, L., 2003. A study of applying genetic programming to reservoir trophic state evaluation using remote sensor data. Int. J. Remote Sens. 24 (11), 2265–2275. https://doi.org/10.1080/01431160210154966.

Chicco, D., Warrens, M.J., Jurman, G., 2021. The coefficient of determination R-squared is more informative than SMAPE, MAE, MAPE, MSE and RMSE in regression analysis evaluation. PeerJ Comput. Sci. 7, e623.

Dillaha, T.A., Beasley, B.D., 1983. Distributed parameter modeling of sediment movement and particle size distributions. Trans. ASAE, ASAE 26 (16), 1766–1772. https://doi.org/10.13031/2013.33840.

Ferreira, C., 2002. Gene Expression Programming in Problem Solving. In: Roy, R., Köppen, M., Ovaska, S., Furuhashi, T., Hoffmann, F. (Eds.), Soft Computing and Industry. Springer London, London, pp. 635–653.

Franco, D.F., 2000. Discipulus TM Software Owner's Manual, Version 3.0 Register Machine. Learning Technologies Inc, Littleton, Colorado.

Ghavidelfar, S., Alvankar, R., Razmkhah, A., 2011. A comparison of the lumped and quasi-distributed clark runoff models in simulating flood hydrographs on a semi-arid watershed. Water Resour. Manage. 25, 1775–1790. https://doi.org/10.1007/s11269-011-9774-5.

Green, W.H., Ampt, G.A., 1911. Studies in soil physics. J. Agric. Sci. 4 (1), 1–24. https://doi.org/10.1017/S0021859600001441.

Guven, A., 2009. Linear genetic programming for time-series modeling of daily flow rate. J. Earth Syst. Sci. 118 (2), 137–146. https://doi.org/10.1007/s12040-009-0022-9.

Hosseini, M., 2014. Water balance simulation of Garahsou basin of Kermanshah province by using SWAT model. J. Watershed Eng. Manage. 6, 63–73 in Persian.

IPCC, (2001). Climate change: The scientific Basis, Contribution of working Group to the Third Assessment Report of the intergovernmental Panell on climate change. Cambridge Univ. Perss, New York, NY, USA, 881 P.

IPCC, (2021). Summary for Policymakers. In: *Climate Change 2021: The Physical Science Basis. Contribution of Working Group I to the Sixth Assessment Report of the Intergovernmental Panel on Climate Change* [Masson-Delmotte, V., P. Zhai, A. Pirani, S. L. Connors, C. Péan, S. Berger, N. Caud, Y. Chen, L. Goldfarb, M. I. Gomis, M. Huang, K. Leitzell, E. Lonnoy, J.B.R. Matthews, T. K. Maycock, T. Waterfield, O. Yelekçi, R. Yu and B. Zhou (eds.)]. Cambridge University Press.

IPCC-TGCIA, (1999). Guidelines on the use of scenario data for climate impact and adaptation assessment. eds. Carter, T.R., Hulme, M. and Lal, M., Version 1, 69pp. Intergovernmental Panel on Climate Change, Task Group on Scenarios for Climate Impact Assessment.

Jakeman, A.J., Hornberger, G.M., 1993. How much complexity is warranted in a rainfall-runoff model? Water Resour. Res. 29 (8), 2637–2649. https://doi.org/10.1029/93WR00877.

Jeong, J., Kannan, N., Arnold, J., Glick, R., Gosselink, L., Srinivasan, R., 2010. Development and integration of sub-hourly rainfall-runoff modeling capability within a watershed model. Water Resour. Manag. 24, 4505–4527. https://doi.org/10.1007/s11269-010-9670-4.

Kennedy, J. (1998). "The Behavior of Particles". In: Porto V.W., Saravanan N., Waagen D., Eiben A.E. (eds) Evolutionary Programming VII. EP 1998. Lecture Notes in Computer Science, vol 1447. Springer, Berlin, Heidelberg, DOI: 10.1007/BFb0040809.

Koza, J.R., 1992. Genetic Programming: on the programming of computers by means of natural selection. Stat. Comput. 4, 87–112. https://doi.org/10.1007/BF00175355.

Lane, M.E., Kirshen, P.H., Vogel, R.M., 1999. Indicators of impact of global climate change on U.S. water resources. J. Water Resour. Plan. Manage. 125 (4), 194–204. https://doi.org/10.1061/(ASCE)0733-9496(1999)125:4(194).

Li, K.Y., Coe, M.T., Ramankutty, N., Jong, R.D., 2007. Modeling the hydrological impact of land-use change in West Africa. J. Hydrol. 337 (3-4), 258–268. https://doi.org/10.1016/j.jhydrol.2007.01.038.

Lin, B., Chen, X., Yao, H., Chen, Y., Liu, M., Gao, L., James, A., 2015. Analyses of land use change impacts on catchment runoff using different time indicators based on SWAT model. Ecol. Ind. 58, 55–63. https://doi.org/10.1016/j.ecolind.2015.05.031.

Liong, S.Y., Gautam, T.R., Khu, S.T., Babovic, V., Keijzer, M., Muttil, N., 2002. Genetic programming, A new paradigm in rainfall runoff modeling. J. Am. Water Resour. Assoc. 38 (3), 705–718. https://doi.org/10.1111/j.1752-1688.2002.tb00991.x.

Littlewood, I.G., Jakeman, A.J., 1994. A new method of rainfall-runoff modelling and its applications in catchment hydrology. Environ. Model. Comput. Mech. Publ. Southampton 2, 143–171.

McCuen, R.H. (2002). Modeling hydrologic change: statistical methods, Lewis Publishers, Dept. of Civil and Environmental Engineering, University of Maryland, 433p.

McCuen, R.H., Knight, Z., Cutter, A.G., 2006. Evaluation of the nash-sutcliffe efficiency index. J. Hydrol. Eng. 11 (6), 597–602.

Mengistu, K.T. (2009). "Watershed Hydrological Responses to Changes in Land Use and Land Cover, and Management Practices at Hare Watershed, Ethiopia", Doctoral Thesis, Universität Siegen, Fakultät Bauingenieurwesen, Research Institute for water and Environment.

Mishra, A., Froebrich, J., Gassman, P.W., 2007. Evaluation of the SWAT model for assessing sediment control structures in a small watershed in India. Trans. ASABE (Am. Soc. Agric. Biol. Eng.) 50 (2), 469–477. https://doi.org/10.13031/2013.22637.

Mitchell, T.D., 2003. Pattern scaling: An examination of the accuracy of the technique for describing future climates. Clim. Change 60 (3), 217–242.

Moghadam, S.H., Ashofteh, P.-S., Loáiciga, H.A., 2019. Application of climate projections and Monte Carlo approach for the assessment of future river flow: Case study of the Khorramabad River basin, Iran. J. Hydrol. Eng. 24 (7) https://doi.org/10.1061/(ASCE)HE.1943-5584.0001801.

Nikolaidis, N.P., Bouraoui, F., Bidoglio, G., 2013. Hydrologic and geochemical modeling of a karstic Mediterranean watershed. J. Hydrol. 477 (4), 129–138. https://doi.org/10.1016/j.jhydrol.2012.11.018.

Richardson, C.W., 1981. Stochastic simulation of daily precipitation, temperature, and solar radiation. Water Resour. Res. 17 (1), 182–190. https://doi.org/10.1029/WR017i001p00182.

Richardson, C.W., Wright, D.A. (1984). WGEN: a model for generating daily weather variables, Report, United States Department of Agriculture, Agriculture Research Service, ARS-8. 83p.

Rostamian, R., Jaleh, A., Afyuni, M., Mousavi, S.F., Heidarpour, M., Jalalian, A., Abbaspour, K.C., 2008. Application of a SWAT model for estimating runoff and sediment in two mountainous basins in central Iran. J. Hydrol. 53 (5), 977–988. https://doi.org/10.1623/hysj.53.5.977.

Sao, D., Kato, T., Tu, L.H., Thouk, P., Fitriyah, A., Oeurng, Ch., 2020. Evaluation of Di_erent objective functions used in the SUFI-2 calibration process of SWAT-CUP on water balance analysis: a case study of the Pursat River Basin, Cambodia. Water 12, 2901. https://doi.org/10.3390/w12102901.

Sarzaeim, P., Bozorg-Haddad, O., Bozorgi, A., Loáiciga, H.A., 2017. Runoff projection under climate change conditions with data-mining methods. J. Irrig. Drain. Eng. 143 (8) https://doi.org/10.1061/(ASCE)IR.1943-4774.0001205.

Semenov, M.A., Barrow, E.M. (1997). LARS-WG a stochastic weather generator for use in climate impact studies. User's manual.

Shi Y., Eberhart R. (1998). "Parameter Selection in Particle Swarm Optimization". In: Porto V.W., Saravanan N., Waagen D., Eiben A.E. (eds) Evolutionary Programming VII. EP 1998. Lecture Notes in Computer Science, vol 1447. Springer, Berlin, Heidelberg, DOI: 10.1007/BFb0040810.

Shi, Y., Eberhart, R. (1999). "Empirical study of particle swarm optimization". Proceeding IEEE International Congerss on Evolutionary Computation. Piscataway, NJ. 1945-1950, DOI: 10.1109/CEC.1999.785511.

Sommerlot, A.R., Nejadhashemi, A., Woznicki, S.A., Giri, S., Prohaska, M.D., 2013. Evaluating the capabilities of watershed-scale models in estimating sediment yield at field-scale. J. Environ. Manage. 127, 227–236. https://doi.org/10.1016/j.jenvman.2013.05.018.

Stöckle, C.O., Campbell, G.S., Nelson, R. (1999). ClimGen manual, Biological Systems Engineering Department, Washington State University, Pullman, WA, 28p.

Te Linde, A.H., Aerts, J.C., Hurkmans, R.T., Eberle, M., 2008. Comparing model performance of two rainfallrunoff models in the Rhine basin using different atmospheric forcing data sets. Hydrol. Earth Syst. Sci. 12 (3), 943–957. https://doi.org/10.5194/hess-12-943-2008.

Tezel, G., Buyukyildiz, M., 2016. Monthly evaporation forecasting using artificial neural networks and support vector machines. Theor. Appl. Climatol. 124, 69–80. https://doi.org/10.1007/s00704-015-1392-3.

Thiery, F., Grieu, S., Traoré, A., Barreau, M., Polit, M., 2008. Integration of neural networks in a geographical information system for the monitoring of a catchment area. Math. Comput. Simul 76 (5-6), 388–397.

Ustoorikar, K., Deo, M.C., 2008. Filling up gaps in wave data with genetic programming. Mar. Struct. 21 (2–3), 177–195. https://doi.org/10.1016/j.marstruc.2007.12.001.

Vale, M., Holman, I.P., 2009. Understanding the hydrological functioning of a shallow lake system within a coastal karstic aquifer in Wales, UK. J. Hydrol. 376 (1–2), 285–294. https://doi.org/10.1016/j.jhydrol.2009.07.041.

van Vuuren, D.P., Edmonds, J., Kainuma, M., Riahi, K., Thomson, A., Hibbard, K., Hurtt, G.C., Kram, T., Krey, V., Lamarque, J.-F., Masui, T., Meinshausen, M., Nakicenovic, N., Smith, S.J., Rose, S.K., 2011. The representative concentration pathways: an overview. Clim. Change 109 (1-2), 5–31.

Vanuytrecht, E., Raes, D., Willems, P., Geerts, S., 2012. Quantifying field-scale of elevated carbon dioxide concentration on crops. Climate Res. 54 (1), 35–47. https://doi.org/10.3354/cr01096.

Wilby, R.L., Harris, I., 2006. A framework for assessing uncertainties in climate change impacts: low flow scenarios for the River Thames, UK. Water Resour. Res. 42 (2), 1–10.

Ye, W., Bates, B.C., Viney, N.R., Sivapalan, M., Jakeman, A.J., 1997. Performance of conceptual rainfall-runoff models in low-yielding ephemeral catchments. Water Resour. Res. 33 (1), 153–166. https://doi.org/10.1029/96WR02840.

Kennedy, J., Eberhart, R. (1995). "Particle Swarm Optimization", In: Sammut C., Webb G.I. (eds) Encyclopedia of Machine Learning. Springer, Boston, MA, DOI: 10.1007/978-0-387-30164-8_630.

Zuo, D., Xu, Z., Yao, W., Jin, S., Xiao, P., Ran, D., 2016. Assessing the effects of changes in land use and climate on runoff and sediment yields from a watershed in the Loess Plateau of China. Sci. Total Environ. 544, 238–250. https://doi.org/10.1016/j.scitotenv.2015.11.060.